Journal of Materials Chemistry C

PAPER

View Article Online
View Journal | View Issue

Cite this: J. Mater. Chem. C, 2017, 5, 2852

Phenyl substitution in tetracene: a promising strategy to boost charge mobility in thin film transistors†

Wenjun Xu,[a] Yaowu He,[a] Imran Murtaza,[bc] Dongwei Zhang,[a] Aiyuan Li,[a] Zhao Hu,[a] Xingwei Zeng,[a] Yitong Guo,[a] Yanan Zhu,[a] Ming Liu[a] and Hong Meng*[ab]

Received 25th October 2016,
Accepted 17th February 2017

DOI: 10.1039/c6tc04624j

rsc.li/materials-c

Tetracene, one of the polyacene derivatives, shows eminent optical and electronic properties with relatively high stability. To take advantage of the intrinsic properties of the tetracene molecule and explore new semiconductors, herein, we report the design and synthesis of two novel p-channel tetracene derivatives, 2-(4-dodecyl-phenyl)-tetracene (C12-Ph-TET) and 2-phenyl-tetracene (Ph-TET). Top contact OTFTs were fabricated using these two materials as semiconductor layers, with charge mobilities up to 1.80 $cm^2 V^{-1} s^{-1}$ and 1.08 $cm^2 V^{-1} s^{-1}$, respectively. Our molecular modeling results indicate that the introduction of phenyl into tetracene can improve the efficient charge transport in electronic devices as a result of the increased electronic coupling between the two neighboring planes of the molecules. AFM images of the thermally evaporated thin films of these two materials show large grains, which correspond to the high mobilities of these devices. Consequently, the mobility of our OTFTs based on C12-Ph-TET is the highest for OTFTs based on tetracene derivatives reported to date. The single crystal analyses show the existence of π–π stacking interactions within the molecules with the introduction of mono-phenyl substituents, which is the main cause of the increased mobility. The impressive properties of these two materials indicate that the introduction of alkyl-phenyl and phenyl group could be an excellent method to improve the properties of the organic semiconductor materials.

1. Introduction

With their scientific and technological development, organic thin-film transistors (OTFTs) have enticed the industry because of their potential applications in organic electronic products such as active matrix organic light-emitting diodes, organic sensors, radio-frequency identification tags and many others.[1–4] Different structures of organic semiconductors have been developed in the recent years such as organic semiconductors based on anthracene[5–9] and pentacene[10–13] derivatives, benzothieno[3,2-*b*]benzothiophene (BTBT) core-based structures,[14–18] and so on. Polyacene derivatives such as tetracene, pentacene and anthracene have been widely investigated as semiconductor materials for organic thin film transistors. However, tetracene provides a better trade-off between stability and charge transfer properties compared to pentacene and anthracene because of its significantly lower rate of decomposition and larger π-conjugation system.[19] The mobility of OTFTs based on tetracene thin films has reached up to 0.12 $cm^2 V^{-1} s^{-1}$,[20] and the single crystal OTFTs have achieved 2.4 $cm^2 V^{-1} s^{-1}$.[21] Because of its high external quantum efficiency, the single crystal of tetracene has also been used in the fabrication of organic light-emitting field-effect transistors.[22,23] Rubrene, one of the most admirable tetracene derivatives, has shown good performance as a single crystal semiconductor in OTFTs[24] and has been used in light-emitting organic field effect transistors as well because of its remarkable optoelectronic properties.[23] In addition, rubrene has shown a very high intrinsic mobility of 40 $cm^2 V^{-1} s^{-1}$,[25] divulging the absolute potential for fabricating high mobility OTFTs based on tetracene derivatives.

Though the single crystal OTFTs based on tetracene have shown higher mobility than amorphous silicon TFTs and the rubrene single-crystal has shown a very high intrinsic mobility, the defect-free single crystals are not easy to fabricate. As a result, OTFTs based on single crystal tetracene are not practical

[a] School of Advanced Materials, Peking University Shenzhen Graduate School, Shenzhen, 518055, China. E-mail: menghong@pkusz.edu.cn
[b] Key Laboratory of Flexible Electronics (KLOFE) & Institute of Advanced Materials (IAM), Jiangsu National Synergetic Innovation Center for Advanced Materials (SICAM), Nanjing Tech University (Nanjing Tech), 30 South Puzhu Road, Nanjing 211816, China
[c] Department of Physics, International Islamic University, Islamabad 44000, Pakistan

† Electronic supplementary information (ESI) available. CCDC 1481132. For ESI and crystallographic data in CIF or other electronic format see DOI: 10.1039/c6tc04624j

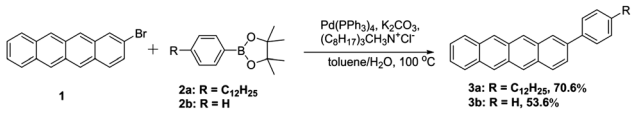

Scheme 1 Synthesis of C12-Ph-TET and Ph-TET.

for large-scale applications. Moreover, the mobility of OTFTs based on tetracene fabricated by thermal evaporation is not high enough. The highest mobility obtained in normal self-assembled monolayers (SAMs) modified OTFTs based on different tetracene derivatives is 0.5 $cm^2 V^{-1} s^{-1}$ (Table S1, ESI†),[26–33] which was achieved by Jeffrey A. Merlo *et al.*[32]

For tuning properties and improving the performance of organic semiconductors, expansion of π-conjugation and introduction of alkyl chain are two vital methods, which are further proven by the examples of BTBT derivatives.[14,34,35] A series of reports demonstrate that the introduction of long alkyl substituent groups leads to higher mobility of OTFTs based on BTBT derivatives.[14,34,35] The morphology of the thin films, one of the most important contributing factors to the stability and repeatability of the OTFTs, has a stringent correlation with molecular planarity, which has been established by a series of experiments.[36,37]

In this context, to maintain the advantages and improve the performance of tetracene, we introduced 4-dodecyl-phenyl and the phenyl group into the tetracene molecule as substituents and report an efficacious synthesis of 2-(4-dodecyl-phenyl)-tetracene (C12-Ph-TET) and 2-phenyl-tetracene (Ph-TET) as new kinds of OTFT semiconductor materials. C12-Ph-TET and Ph-TET were synthesized by Suzuki coupling, as shown in Scheme 1. OTFT devices were fabricated using these two materials as active layers, showing the highest charge mobilities up to 1.80 $cm^2 V^{-1} s^{-1}$ and 1.08 $cm^2 V^{-1} s^{-1}$, respectively. To the best of our knowledge, the mobility of OTFTs based on C12-Ph-TET is the highest value amid OTFTs based on tetracene derivatives reported until now. The properties of these two materials clearly demonstrate that the introduction of 4-dodecyl-phenyl and phenyl could be a virtuous method to improve the properties of organic semiconductor materials. This conclusion is also supported by our computational modeling results presented in the next section.

2. Results and discussion

2a. Synthesis

The 2-bromo-tetracene was synthesized according to a delivered patent,[38] and 2-(4-dodecyl-phenyl)-4,4,5,5-tetramethyl-[1,3,2]-dioxaborolane was synthesized according to the literature.[39] The C12-Ph-TET and Ph-TET were both synthesized by Pd-mediated Suzuki coupling, allowing the reaction at 100 °C under vigorous stirring for 2 days. Details of the synthetic routes are reported in the ESI.†

2b. Optical and electrochemical properties

C12-Ph-TET and Ph-TET show nearly the same absorption peaks in both the thin film and solution states (Fig. 1a). The manifestation of this phenomenon could be due to the same π-conjugation

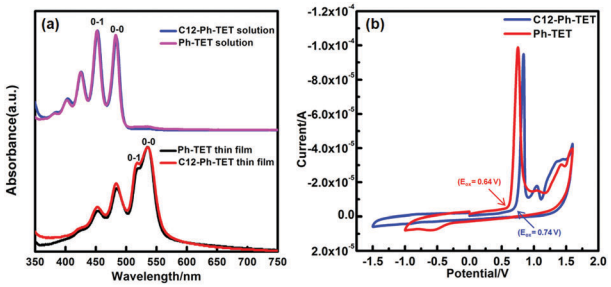

Fig. 1 (a) Normalized UV-vis absorption spectra of C12-Ph-TET and Ph-TET in the thin film and solution states. (b) Cyclic voltammetry (CV) curves of C12-Ph-TET and Ph-TET. The oxidation potential is obtained at the onset of the cyclic voltammogram.

system in these two compounds. The onset of UV absorption for both the thin films occurs at the wavelength of 562 nm, and the maximum absorption peaks appear at the wavelength of 536 nm. However, in the solution state of both of the materials, the absorption onset appears at the wavelength of 500 nm. The UV data reveal the fact that the substitution of long alkyl chains has little influence on the UV absorption peaks. The absorption peaks at the wavelengths of 451, 483 and 536 nm in the thin film state may be ascribed to the π–π* transition of the localized tetracene core and the phenyl substituent. The bathochromic shift and the increase in the ratio of the vibronic peak intensities between the 0–0 and 0–1 peaks of the absorption spectra in the thin film state compared to that in the solution state are strong evidence for the J-aggregation in the thin films.[40] By comparing the absorption peaks of the C12-Ph-TET and Ph-TET thin films, we can make a conclusion that the introduction of the long dodecyl chain does not have a profound influence on the UV absorption of the thin films. This result is different from the published experiments,[34] and it shows that the introduction of the long alkyl chain makes a trivial contribution to disturbing the aggregation of the aromatic part of the molecule.

The normalized UV-vis absorption spectra indicate the optical bandgap of the materials, which can be calculated from the absorption onset wavelength. The calculated result of the optical bandgap (E_{opt}) is 2.21 eV for both the materials. Fig. 1b shows the cyclic voltammograms of the C12-Ph-TET and Ph-TET thin films. The first oxidation peak values of C12-Ph-TET and Ph-TET, used in the calculation of the HOMO level, appear at 0.74 and 0.64 V, respectively, using ferrocene as the inner standard. The calculated values for C12-Ph-TET and Ph-TET are: $E_{HOMO} = -5.46$ eV and -5.36 eV, $E_{LUMO} = -3.25$ eV and -3.15 eV, respectively. In the literature, both the HOMO and LUMO levels have been calculated from cyclic voltammograms.[41] However, we could not directly obtain the LUMO energy level from the cyclic voltammograms, as there are no reductive peaks in the graphs. The LUMO levels were calculated by using the equation: $E_{LUMO} = E_{HOMO} + E_{opt}$.[42–44] The electronic properties of C12-Ph-TET and Ph-TET are summarized in Table 1.

2c. Crystal structure

In order to correlate the transport properties with the packing structure of the molecules in the condensed phase, we performed

Table 1 Electronic properties of C12-Ph-TET and Ph-TET

Compound	λ_{edge}[a]/nm	E_g[b]/eV	E_{HOMO}[c]/eV	E_{LUMO}[d]/eV
C12-Ph-TET	562	2.21	−5.46	−3.25
Ph-TET	562	2.21	−5.36	−3.15

[a] From ultraviolet absorption spectra of these two compounds (thin film). [b] Calculated by λ_{edge}/nm of ultraviolet absorption spectrum (thin film) using the equation: $1240/\lambda_{onset}$. [c] From cyclic voltammetry data *vs.* Fc/Fc^+ of these two compounds using equation HOMO = $-[E_{ox} - E_{(Fc/Fc^+)} + 4.8]$ (eV). [d] Calculated by E_g and E_{HOMO} using equation $E_{LUMO} = (E_{HOMO} + E_{opt})$ (eV).[42–44]

single crystal X-ray analysis. We successfully attained single crystals of Ph-TET by physical vapor transport. Depicted in Fig. 2 are the molecular and packing structures of Ph-TET demonstrating that the single crystal of Ph-TET is a monoclinic crystal belonging to the $P2_1$ space group with crystal parameters of a = 6.1567(7) Å, b = 7.2515(8) Å and c = 16.757(2) Å, whereas the crystal structure of tetracene is triclinic (Fig. S1, ESI†). The distance between the two H-atoms of the phenyl and neighboring tetracene molecules is about 2.606 Å (Fig. 2a), and the distance between the two H-atoms of the neighboring tetracene cores is 2.754 Å (Fig. S1a, ESI†). The shorter the distance between the two neighboring atoms, the more the enhancement of the overlay electronic coupling, which favors the charge transport. To facilitate a deeper understanding of the

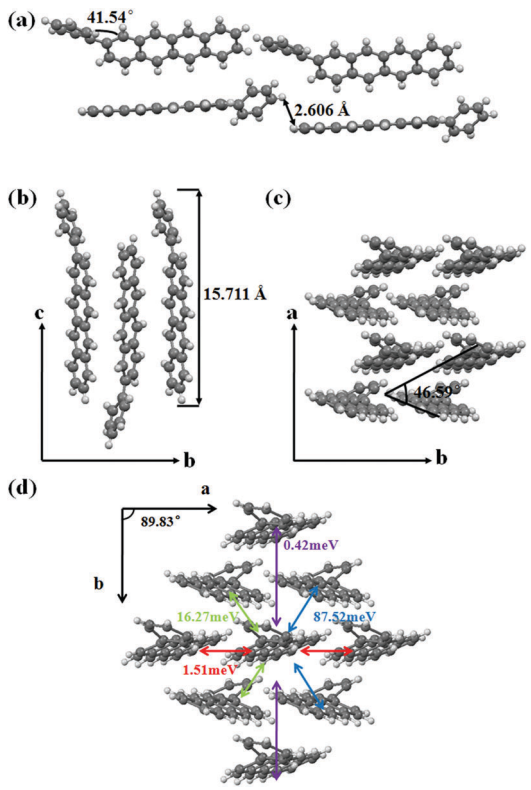

Fig. 2 Molecular structure, shortest intermolecular distance between two H-atoms and torsion angle between tetracene and phenyl planes (a), packing pattern and molecular length of Ph-TET projected along the crystallographic *a*-axis (b), *c*-axis projection showing the herringbone structure and dihedral angle between the two tetracene planes of Ph-TET (c), charge transfer integrals in the single crystal of Ph-TET molecules (d).

phenyl substitution on the semiconductor properties, the charge transfer integrals were calculated using the software Amsterdam Density Functional (ADF). The software uses a generalized gradient approximation with the PW91 functional and the basis set of triple-Z 2 plus polarization function (GGA: PW91/TZ2P) for modeling the charge transfer properties by utilizing the single crystal structure of the organic semiconductor materials. The charge transfer integrals of Ph-TET were calculated for the adjacent molecules along their π–π stacking direction, which resulted in a charge transfer integral of about 87.52 meV (Fig. 2d), and this is much higher than that of the tetracene (70.15 meV, Fig. S1d, ESI†). This theoretical result predicts that the phenyl substitution has a positive influence on the improvement of the hole mobility of tetracene and is supplemented by our experimental results as well. Moreover, we found that the dihedral angle between the two tetracene planes is 51.38° (Fig. S1c, ESI†), and the angle between the two tetracene planes of Ph-TET is 46.59° (Fig. 2c). This is another contributing factor towards increased mobility because a smaller angle between the two neighboring planes of the molecule creates more overlap of the electronic coupling and a higher mobility. The packing structures of Ph-TET are also shown in Fig. 2, portraying the mean angle of 46.59° between the tetracene planes and the molecular arrangement pattern of Ph-TET as a typical herringbone motif (Fig. 2c). The interlayer spacing (*d*-spacing) between the tetracene planes calculated by the single crystal XRD data is 16.757 Å. We were lucky to obtain the single crystal XRD data; however, the quality of the single crystals was not good enough to fabricate single crystal OTFTs.

2d. Morphological characterization

X-ray diffraction (XRD) data and atomic force microscope (AFM) images were obtained to reveal the morphology of the thin films deposited by thermal evaporation on the *n*-octyltrichlorosilane (OTS)-treated Si/SiO_2 substrate. Thin films of C12-Ph-TET were deposited on the substrates at room temperature, 60 °C and 100 °C, whereas the thin films of Ph-TET were deposited at room temperature and 60 °C because the efforts to deposit Ph-TET at 100 °C were unsuccessful. The XRD results show that the thin films of Ph-TET fabricated at 60 °C are far more crystallized than the thin films fabricated at room temperature, as there are higher incisive peaks in the XRD data. This result reveals that Ph-TET has an excellent oriented-growth property. The incisive peak at $2\theta = 5.5°$ can be assigned to the (0 0 1) reflection, and a *d*-spacing of 15.82 Å can be calculated using Bragg's equation, which is comparable to the value calculated by single crystal XRD. Four reflection peaks appearing at 5.47, 10.74, 16.01, 21.33 can be assigned to (0 0 1), (0 0 2), (0 0 3) and (0 0 4) based on the single crystal XRD data of Ph-TET. From the single crystal and thin film XRD *d*-spacing results, we can conclude that the Ph-TET has an edge-on orientation to the substrate surface. However, the XRD data of C12-Ph-TET are rather diverse. The XRD data of the C12-Ph-TET thin films fabricated at 100 °C show higher incisive peaks at 3.0° than the thin films fabricated at room temperature and 60 °C, which show higher crystallization of the thin films fabricated at 100 °C (Fig. 3). Meanwhile, a new peak at 4.4° appears as the substrate temperature rises to 100 °C,

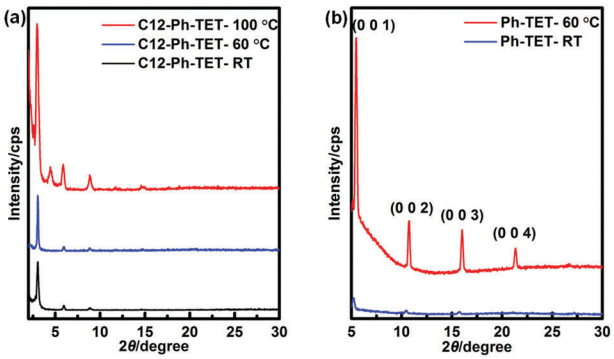

Fig. 3 XRD data of C12-Ph-TET (a) and Ph-TET (b) thin films fabricated by thermal evaporation.

which also reveals a better crystallinity in the thin films and perhaps reveals the formation of a new phase.[45]

The results demonstrate that there is obvious molecular orientation in the thin films, which is also portrayed by the AFM images. To further probe the morphology of C12-Ph-TET and Ph-TET thin films fabricated by thermal evaporation at different substrate temperatures, atomic force microscope (AFM) was utilized. The AFM images shown in Fig. 4 depict that the thin films of the two synthesized compounds have totally different morphologies. For C12-Ph-TET, the thin films fabricated on the substrate at room temperature (Fig. 4a) show no big grains, while those fabricated on the substrate at 60 °C show small grains (Fig. 4b). However, the thin films fabricated at 100 °C show big grains in the AFM images (Fig. 4c). The AFM results are also consistent with the mobility values, and it has been proven by a series of experiments that big grain size makes an enormous contribution to higher mobility.[36,37] The same conclusion could be drawn to elucidate the data we obtained for the thin films of Ph-TET. Ph-TET thin films fabricated on the substrate at both the room temperature (Fig. 4d) and 60 °C (Fig. 4e) show big crystalline sizes, which increase with the substrate temperature. We can also make a conclusion that for the long alkyl chain compound C12-Ph-TET, high substrate temperature has a beneficial influence on the growth of the grain size and does not change the molecular orientation much.

The molecular length of Ph-TET is 15.711 Å (Fig. 2b), which was calculated using the single crystal XRD data. Comparing the molecular length with the AFM step value, which is around 16 Å (Fig. S4, ESI†), it can be deduced that the compound Ph-TET adopts a layer-by-layer configuration on the wafers. By making a comparison between these two materials, we can deduce that the long alkyl chain increases the grain size of the

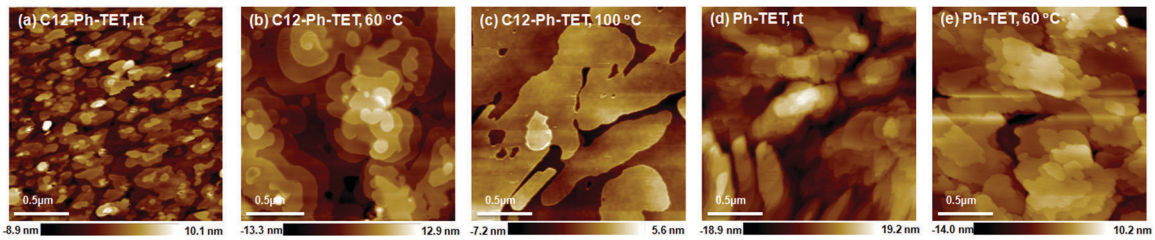

Fig. 4 AFM images of C12-Ph-TET and Ph-TET thin films fabricated by thermal evaporation. (a) C12-Ph-TET, substrate: room temperature; (b) C12-Ph-TET, substrate: 60 °C; (c) C12-Ph-TET, substrate: 100 °C; (d) Ph-TET, substrate: room temperature; (e) Ph-TET, substrate: 60 °C.

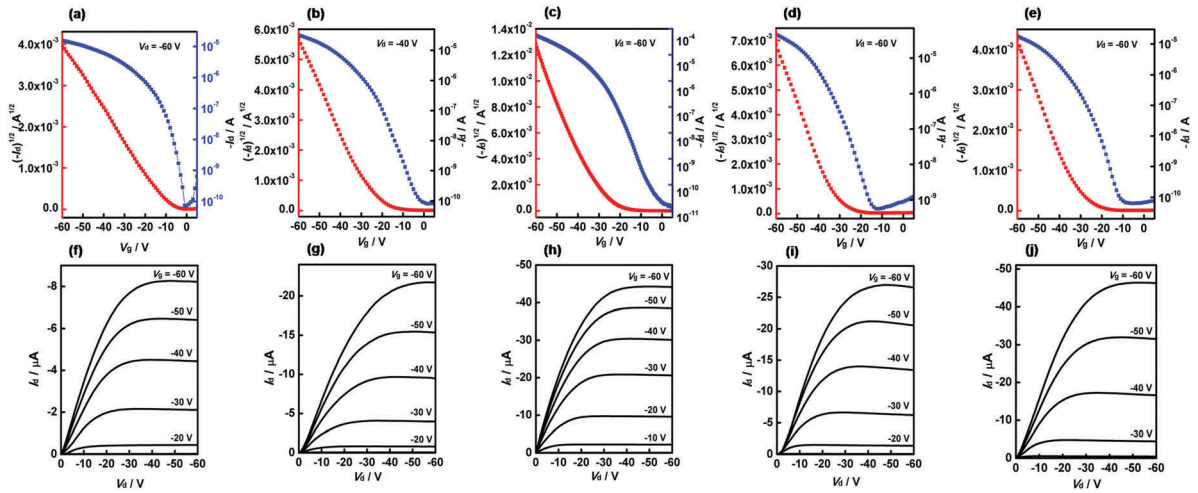

Fig. 5 Transfer curves of (a) C12-Ph-TET, substrate: room temperature; (b) C12-Ph-TET, substrate: 60 °C; (c) C12-Ph-TET, substrate: 100 °C; (d) Ph-TET, substrate: room temperature; (e) Ph-TET, substrate: 60 °C and output curves of (f) C12-Ph-TET, substrate: room temperature; (g) C12-Ph-TET, substrate: 60 °C; (h) C12-Ph-TET, substrate: 100 °C; (i) Ph-TET, substrate: room temperature; (j) Ph-TET, substrate: 60 °C.

Table 2 OTFT properties of C12-Ph-TET and Ph-TET

Compound	T_{sub}/°C	μ_{OTFT}[a]/cm^2 V^{-1} s^{-1}	I_{on}/I_{off}[b]	V_T[c]/V
C12-Ph-TET	rt	0.11 (0.08 ± 0.02)	(8.27 ± 7.02) × 10^4	−7.7 ± 1.8
	60	0.33 (0.22 ± 0.07)	(9.57 ± 5.13) × 10^5	−15.2 ± 1.8
	100	1.80 (1.63 ± 0.11)	(6.80 ± 3.71) × 10^6	−18.7 ± 2.5
	120	0.45 (0.33 ± 0.11)	(3.15 ± 2.81) × 10^5	−12.2 ± 2.2
Ph-TET	rt	0.52 (0.35 ± 0.09)	(1.00 ± 0.36) × 10^7	−16.6 ± 2.2
	60	1.08 (0.69 ± 0.20)	(1.71 ± 0.58) × 10^6	−21.2 ± 2.5

[a] Values without brackets are the highest mobilities of the devices, and values within brackets are average values of 10 devices. [b] Average on/off ratio value of 10 devices. [c] Average threshold voltage value of 10 devices.

thin films more effectively when the substrate temperature is high enough. This phenomenon could be explained by the molecular arrangement effect of the long alkyl chain.

2e. OTFT properties

The bottom-gate top-contact OTFT devices were fabricated by thermal evaporation and evaluated under ambient conditions. OTFTs based on C12-Ph-TET and Ph-TET show typical p-type transfer and output characteristics as shown in Fig. 5. It can be seen in Table 2 that mobilities of the devices based on both C12-Ph-TET and Ph-TET are higher than the thin film OTFTs based on tetracene,[19,46–48] and the mobility results supplement our XRD and AFM data very well. The average mobility of ten devices based on C12-Ph-TET is 1.63 cm^2 V^{-1} s^{-1}, and the highest value obtained was 1.80 cm^2 V^{-1} s^{-1}. Whereas, ten devices based on Ph-TET accomplished an average mobility of 0.69 cm^2 V^{-1} s^{-1} and the highest value of 1.08 cm^2 V^{-1} s^{-1}. As shown in Table 2, we can easily find that the mobility of the phenyl-dodecyl substituent tetracene derivative is extremely responsive to the substrate temperature. This result reveals the fact that the properties of the OTFTs based on long alkyl derivatives can be controlled by altering the substrate temperature. This remarkable performance makes C12-Ph-TET one of the best tetracene derivatives. Moreover, our OFETs show high threshold voltages, which may be due to the fact that the HOMO level of C12-Ph-TET (−5.46 eV) and Ph-TET (−5.36 eV) does not match well with the work function of gold (−5.1 eV), and secondly the charge trap states limit the charge injection. In order to check the operational stability of the OTFT devices, we obtained transfer characteristics for 100 sweep cycles in ambient conditions, and the data showed no obvious changes (Fig. S7, ESI†).

3. Conclusions

In conclusion, we discovered two new phenyl-tetracene derivatives, 2-(4-dodecyl-phenyl)-tetracene and 2-phenyl-tetracene, and studied their optical and electrochemical properties. OTFTs based on these two materials were fabricated and presented the highest charge mobilities, up to 1.80 cm^2 V^{-1} s^{-1} and 1.08 cm^2 V^{-1} s^{-1}. These two values are higher than the other reported tetracene derivatives. We also systematically analyzed the structural and morphological data of the thin films fabricated from these two materials and found that the mobilities of the devices remarkably supplement the morphology of the thin films. It is observed that the two substituent groups dramatically enhance the charge carrier mobility of tetracene. The single crystal analyses provide a simple means of understanding crystal effects and show that regardless of the twisting caused by the phenyl substituent, π–π stacking interactions take place within the molecules that are in accord with the increase in mobility. By utilizing the single crystal data, we calculated the charge transfer integrals of Ph-TET and tetracene. The integrals clearly demonstrate that the introduction of phenyl into tetracene can improve the efficient charge transport in electronic devices as a result of the increased electronic coupling between the two neighboring planes of the molecules and consequently has a positive influence on the hole mobility. These results show that the introduction of the phenyl and long alkyl chain group is an exceptional method to fine tune the properties of organic semiconductor materials and has a profound influence on the morphology and grain size of the organic semiconductor thin films, which leads to improved performance in the device. The obtained high mobility phenyl substituted tetracene semiconductors not only provide a new way to improve the device performance but also appended one of the highest organic semiconductor families beyond the recent BTBT derivative tribes.

4. Experimental section

4a. Synthesis and characterization

The organic semiconductor materials C12-Ph-TET and Ph-TET were synthesized by Suzuki coupling.

Synthesis of 2-(4-dodecyl-phenyl)-tetracene. To a 350 mL pressure bottle, 2-bromotetracene (2.5 g, 8.1 mmol), 2-(4-dodecyl-phenyl)-4,4,5,5-tetramethyl-[1,3,2]-dioxaborolane (4.55 g, 12.2 mmol), methyl-trioctylammoniumchloride (1.64 g, 4.05 mmol), tetrakis triphenyl-phosphinepalladium (0.09 g, 0.081 mmol), toluene (40 mL) and 2 mol L^{-1} K_2CO_3 (12.15 mL) were added. After nitrogen-blowing for 20 min, the reacting system was stirred and heated to 100 °C for 48 h. After cooling to room temperature, the sediments were separated by filtration and washed twice with toluene. The crude product was purified by sublimation in a 5-zone furnace to give an orange product (2.71 g, 70.6%).

C12-Ph-TET: ^{1}H NMR ($CDCl_3$, 300 MHz): δ 8.71 (s, 1H), 8.67 (s, 3H), 8.19 (s, 1H), 8.09–7.99 (m, 3H), 7.73–7.70 (m, 3H), 7.42–7.38 (m, 2H), 7.33 (d, 2H, J = 8.0 Hz), 2.69 (m, 2H), 1.69 (m, 2H, CH_2) 1.27 (m, 18H, 9 × CH_2), 0.88 (t, 3H, J = 6.6 Hz). HRMS (APCI), m/z calculated for $C_{36}H_{41}$ $[M + H]^+$: 473.3208.

Found: 473.3204. Structure of the C12-Ph-TET was confirmed by NMR (Bruker, 300 MHz) and high resolution mass spectrum (HRMS).

We could not obtain the ^{13}C NMR data of C12-Ph-TET due to its low solubility.

Synthesis of 2-phenyl-tetracene. To a 350 mL pressure bottle, 2-bromotetracene (2.5 g, 8.1 mmol), phenyl-4,4,5,5-tetramethyl-[1,3,2]-dioxaborolane (2.49 g, 12.2 mmol), methyltrioctylammonium-chloride (1.64 g, 4.05 mmol), tetrakis triphenylphosphine-palladium (0.09 g, 0.081 mmol), toluene (40 mL) and 2 mol L^{-1} K_2CO_3 (12.15 mL) were added. After nitrogen-blowing for 20 min, the reacting system was stirred and heated to 100 °C for 48 h. After cooling to room temperature, the sediments were separated by filtration and washed twice with toluene. The crude product was purified by sublimation in a 5-zone furnace to give an orange product (1.33 g, 53.6%).

Ph-TET: ^1H NMR ($CDCl_3$, 300 MHz): δ 8.75 (s, 1H), 8.70 (s, 3H), 8.23 (s, 1H), 8.12 (d, 1H, J = 9.2 Hz), 8.05–8.02 (m, 2H), 7.84–7.80 (m, 2H, J = 7.1 Hz), 7.75–7.72 (m, 1H), 7.55 (t, 2H, J = 7.5 Hz), 7.46–7.41 (m, 3H). HRMS (APCI), m/z calculated for $C_{24}H_{17}$ $[M + H]^+$: 305.1330. Found: 305.1333.

Structure of the Ph-TET was confirmed by NMR and HRMS.

We could not obtain the ^{13}C NMR data of Ph-TET due to its low solubility.

4b. General procedures and experimental details

Cyclic voltammetry. The C12-Ph-TET and Ph-TET thin films on the platinum electrode were deposited by thermal evaporation. To detect the HOMO and LUMO of the two compounds, 0.1 mol L^{-1} tetrabutylammoniumhexafluorophosphate (Bu_4NPF_6) of anhydrous acetonitrile (CH_3CN) solution was made. After piping nitrogen in the solution for 30 min and keeping the solution in a nitrogen atmosphere, the CV data was obtained at a scan rate of 100 mV s^{-1} using Ag/Ag^+ as the reference electrode (+0.08 V *vs.* Ag/Ag^+ nonaqueous reference electrode). The Ag/Ag^+ electrode was made by soaking a clean Ag wire into a 0.01 mol L^{-1} $AgNO_3$ solution in dry CH_3CN and 0.1 mol L^{-1} tetrabutylammonium-hexafluorophosphate (Bu_4NPF_6).

OTFT devices fabrication. The bottom-gate top-contact OTFT devices were fabricated on the OTS treated n-Si wafers with approximately 200 nm of the SiO_2 layer. In this case, the Si wafers were cleaned by acetone, deionized water and isopropanol at room temperature in the ultrasonic bath for 20 min. After ultrasonic cleaning, the n-doped Si wafers were exposed to ultraviolet radiation for 20 min. Then, the wafers were immersed in the 0.1 mol L^{-1} OTS/toluene solution and heated to 60 °C for 15 min and washed with toluene for 2 times. The residual toluene was dried up by nitrogen gas gun.

The 20 nm thick thin films of the organic semiconductor on the substrate were grown by thermal evaporation at a rate of 0.5 Å s^{-1}. The 50 nm thick gold was used as a source and drain electrode and was also deposited by thermal evaporation at the same rate. The drain–source channel width (W)/length (L) were 400 μm/40 μm, 600 μm/60 μm, 800 μm/80 μm, and 1000 μm/100 μm, respectively.

The bottom-gate top-contact OTFT devices were fabricated by thermal evaporation and evaluated under ambient conditions. The mobilities of the devices were calculated, as shown in Table 2, using the equation:

$$I_D = (W/2L)\mu C_i(V_G - V_T)^2$$

where I_D represents the saturation drain current, L and W symbolize the channel length and channel width, respectively, C_i represents the capacitance of the oxide dielectric layer, and V_G and V_T represent the gate bias voltage and threshold voltage respectively.

Acknowledgements

This work was financially supported by Shenzhen Key Laboratory of Organic Optoelectromagnetic Functional Materials of Shenzhen Science and Technology Plan (ZDSYS20140509094114164), the Shenzhen Peacock Program (KQTD2014062714543296), Shenzhen Science and Technology Research Grant (JCYJ20140509093817690), Nanshan Innovation Agency Grant (No. KC2015ZDYF0016A), Guangdong Key Research Project (No. 2014B090914003, 2015B090914002), Guangdong Talents Project, National Basic Research Program of China (973 Program, No. 2015CB856505), NSFC (51373075), Natural Science Foundation of Guangdong Province (2014A030313800), National Natural Science Foundation of China (Grant No. 51603003), and Shenzhen Science and Technology Research Grant (JCYJ20150629144328079). We thank Dr Mingjian Zhang for the refinement of the single crystal XRD. We also thank Ying Chen and Qian Wu for their help on the growth of single crystals, and we are thankful to Prof. Osamu Goto for his constant support during the development of this article. CCDC 1481132 contains the supplementary crystallographic data for this paper.

Notes and references

1 G. Gelinck, P. Heremans, K. Nomoto and T. D. Anthopoulos, *Adv. Mater.*, 2010, **22**, 3778–3798.
2 A. R. Murphy and J. M. Frechet, *Chem. Rev.*, 2007, **107**, 1066–1096.
3 A. C. Arias, J. D. MacKenzie, I. McCulloch, J. Rivnay and A. Salleo, *Chem. Rev.*, 2010, **110**, 3–24.
4 M. L. Chabinyc and A. Salleo, *Chem. Mater.*, 2004, **16**, 4509–4521.
5 J. Liu, H. Zhang, H. Dong, L. Meng, L. Jiang, L. Jiang, Y. Wang, J. Yu, Y. Sun, W. Hu and A. J. Heeger, *Nat. Commun.*, 2015, **6**, 10032.
6 H. Klauk, U. Zschieschang, R. T. Weitz, H. Meng, T. Sun, G. Nunes, D. E. Keys, C. R. Fincher and Z. Xiang, *Adv. Mater.*, 2007, **19**, 3882–3887.
7 H. Meng, F. Sun, M. B. Goldfinger, F. Gao, D. J. Londono, W. J. Marshal, G. S. Blackman, K. D. Dobbs and D. E. Keys, *J. Am. Chem. Soc.*, 2006, **128**, 9304–9305.
8 H. Meng, F. Sun, M. B. Goldfinger, G. D. Jaycox, Z. Li, W. J. Marshall and G. S. Blackman, *J. Am. Chem. Soc.*, 2005, **127**, 2406–2407.

9 J. Liu, H. Dong, Z. Wang, D. Ji, C. Cheng, H. Geng, H. Zhang, Y. Zhen, L. Jiang, H. Fu, Z. Bo, W. Chen, Z. Shuai and W. Hu, *Chem. Commun.*, 2015, **51**, 11777–11779.
10 S. K. Park, T. N. Jackson, J. E. Anthony and D. A. Mourey, *Appl. Phys. Lett.*, 2007, **91**, 063514.
11 M. M. Payne, S. R. Parkin, J. E. Anthony, C. C. Kuo and T. N. Jackson, *J. Am. Chem. Soc.*, 2005, **127**, 4986–4987.
12 Y. N. Li, Y. L. Wu, P. Liu, Z. Prostran, S. Gardner and B. S. Ong, *Chem. Mater.*, 2007, **19**, 418–423.
13 G. R. Llorente, M. B. Dufourg-Madec, D. J. Crouch, R. G. Pritchard, S. Ogier and S. G. Yeates, *Chem. Commun.*, 2009, 3059–3061.
14 H. Ebata, T. Izawa, E. Miyazaki, K. Takimiya, M. Ikeda, H. Kuwabara and T. Yui, *J. Am. Chem. Soc.*, 2007, **129**, 15732–15733.
15 Y. Yuan, G. Giri, A. L. Ayzner, A. P. Zoombelt, S. C. Mannsfeld, J. Chen, D. Nordlund, M. F. Toney, J. Huang and Z. Bao, *Nat. Commun.*, 2014, **5**, 3005.
16 H. Iino, T. Usui and J. Hanna, *Nat. Commun.*, 2015, **6**, 6828.
17 H. Iino and J. Hanna, *Adv. Mater.*, 2011, **23**, 1748–1751.
18 Y. He, W. Xu, I. Murtaza, D. Zhang, C. He, Y. Zhu and H. Meng, *RSC Adv.*, 2016, **6**, 95149–95155.
19 J. E. Anthony, *Chem. Rev.*, 2006, **106**, 5028–5048.
20 D. J. Gundlach, J. A. Nichols, L. Zhou and T. N. Jackson, *Appl. Phys. Lett.*, 2002, **80**, 2925–2927.
21 C. Reese, W. J. Chung, M. M. Ling, M. Roberts and Z. N. Bao, *Appl. Phys. Lett.*, 2006, **89**, 202108.
22 T. Takahashi, T. Takenobu, J. Takeya and Y. Iwasa, *Adv. Funct. Mater.*, 2007, **17**, 1623–1628.
23 T. Takenobu, S. Z. Bisri, T. Takahashi, M. Yahiro, C. Adachi and Y. Iwasa, *Phys. Rev. Lett.*, 2008, **100**, 066601.
24 V. Podzorov, E. Menard, A. Borissov, V. Kiryukhin, J. A. Rogers and M. E. Gershenson, *Phys. Rev. Lett.*, 2004, **93**, 086602.
25 J. Takeya, M. Yamagishi, Y. Tominari, R. Hirahara, Y. Nakazawa, T. Nishikawa, T. Kawase, T. Shimoda and S. Ogawa, *Appl. Phys. Lett.*, 2007, **90**, 102120.
26 T. Kimoto, K. Tanaka, M. Kawahata, K. Yamaguchi, S. Otsubo, Y. Sakai, Y. Ono, A. Ohno and K. Kobayashi, *J. Org. Chem.*, 2011, **76**, 5018–5025.
27 T. Kimoto, K. Tanaka, Y. Sakai, A. Ohno, K. Yoza and K. Kobayashi, *Org. Lett.*, 2009, **11**, 3658–3661.
28 T. Okamoto, K. Nakahara, A. Saeki, S. Seki, J. H. Oh, H. B. Akkerman, Z. Bao and Y. Matsuo, *Chem. Mater.*, 2011, **23**, 1646–1649.
29 S. W. Park, J. M. Hwang, J. M. Choi, D. K. Hwang, M. S. Oh, J. H. Kim and S. Ima, *Appl. Phys. Lett.*, 2007, **90**, 153512.
30 M. Mamada, H. Katagiri, T. Sakanoue and S. Tokito, *Cryst. Growth Des.*, 2015, **15**, 442–448.
31 R. Schmidt, S. Gottling, D. Leusser, D. Stalke, A. M. Krause and F. Wurthner, *J. Mater. Chem.*, 2006, **16**, 3708–3714.
32 J. A. Merlo, C. R. Newman, C. P. Gerlach, T. W. Kelley, D. V. Muyres, S. E. Fritz, M. F. Toney and C. D. Frisbie, *J. Am. Chem. Soc.*, 2005, **127**, 3997–4009.
33 F. Cicoira, C. Santato, A. Dadvand, C. Harnagea, A. Pignolet, P. Bellutti, Z. Xiang, F. Rosei, H. Meng and D. F. Perepichka, *J. Mater. Chem.*, 2008, **18**, 158–161.
34 M. J. Kang, I. Doi, H. Mori, E. Miyazaki, K. Takimiya, M. Ikeda and H. Kuwabara, *Adv. Mater.*, 2011, **23**, 1222–1225.
35 T. Izawa, E. Miyazaki and K. Takimiya, *Adv. Mater.*, 2008, **20**, 3388–3392.
36 G. Horowitz and M. E. Hajlaoui, *Adv. Mater.*, 2000, **12**, 1046–1050.
37 A. Di Carlo, F. Piacenza, A. Bolognesi, B. Stadlober and H. Maresch, *Appl. Phys. Lett.*, 2005, **86**, 263501.
38 R. K. Bailey, G. B. Blanchet, J. W. Catron, R. J. Chesterfield, F. Gao, H. D. Glicksman, M. B. Goldfinger, G. D. Jaycox, L. K. Johnson and R. L. Keusseyan, *Thin film transistor comprising novel conductor and dielectric compositions*, US 20080012006 A1, 2008, p. 56.
39 Y. He, M. Sezen, D. Zhang, A. Li, L. Yan, H. Yu, C. He, O. Goto, Y.-L. Loo and H. Meng, *Adv. Electron. Mater.*, 2016, **2**, 1600179.
40 F. C. Spano, *Acc. Chem. Res.*, 2010, **43**, 429–439.
41 J.-L. Bredas, *Mater. Horiz.*, 2014, **1**, 17–19.
42 A. Arjona-Esteban, J. Krumrain, A. Liess, M. Stolte, L. Huang, D. Schmidt, V. Stepanenko, M. Gsänger, D. Hertel, K. Meerholz and F. Würthner, *J. Am. Chem. Soc.*, 2015, **137**, 13524–13534.
43 N. Zhou, X. Guo, R. P. Ortiz, T. Harschneck, E. F. Manley, S. J. Lou, P. E. Hartnett, X. Yu, N. E. Horwitz, P. M. Burrezo, T. J. Aldrich, J. T. López Navarrete, M. R. Wasielewski, L. X. Chen, R. P. H. Chang, A. Facchetti and T. J. Marks, *J. Am. Chem. Soc.*, 2015, **137**, 12565–12579.
44 X. Guo, N. Zhou, S. J. Lou, J. W. Hennek, R. Ponce Ortiz, M. R. Butler, P.-L. T. Boudreault, J. Strzalka, P.-O. Morin, M. Leclerc, J. T. López Navarrete, M. A. Ratner, L. X. Chen, R. P. H. Chang, A. Facchetti and T. J. Marks, *J. Am. Chem. Soc.*, 2012, **134**, 18427–18439.
45 B. Servet, G. Horowitz, S. Ries, O. Lagorsse, P. Alnot, A. Yassar, F. Deloffre, P. Srivastava and R. Hajlaoui, *Chem. Mater.*, 1994, **6**, 1809–1815.
46 R. W. I. de Boer, T. M. Klapwijk and A. F. Morpurgo, *Appl. Phys. Lett.*, 2003, **83**, 4345.
47 S. Bertolazzi, J. Wunsche, F. Cicoira and C. Santato, *Appl. Phys. Lett.*, 2011, **99**, 013301.
48 C. Goldmann, S. Haas, C. Krellner, K. P. Pernstich, D. J. Gundlach and B. Batlogg, *J. Appl. Phys.*, 2004, **96**, 2080–2086.

